Scalable Control Allocation: Real-time Optimized Current Control in the Modular Multilevel Converter for Polyphase Systems

Grégoire Le Goff, Maurice Fadel, Marc Bodson

▶ **To cite this version:**

Grégoire Le Goff, Maurice Fadel, Marc Bodson. Scalable Control Allocation: Real-time Optimized Current Control in the Modular Multilevel Converter for Polyphase Systems. 2022 International Symposium on Power Electronics, Electrical Drives, Automation and Motion (SPEEDAM), Jun 2022, Sorrento, Italy. pp.712-718, 10.1109/SPEEDAM53979.2022.9842095 . hal-03813653

HAL Id: hal-03813653
https://hal.science/hal-03813653

Submitted on 13 Oct 2022

HAL is a multi-disciplinary open access archive for the deposit and dissemination of scientific research documents, whether they are published or not. The documents may come from teaching and research institutions in France or abroad, or from public or private research centers.

L'archive ouverte pluridisciplinaire **HAL**, est destinée au dépôt et à la diffusion de documents scientifiques de niveau recherche, publiés ou non, émanant des établissements d'enseignement et de recherche français ou étrangers, des laboratoires publics ou privés.

Distributed under a Creative Commons Attribution - NonCommercial - NoDerivatives 4.0 International License

Scalable Control Allocation: Real-time Optimized Current Control in the Modular Multilevel Converter for Polyphase Systems

Grégoire Le Goff
LAPLACE
Université de Toulouse, CNRS, INPT, UPS
Toulouse, France
legoff@laplace.univ-tlse.fr

Maurice Fadel
LAPLACE
Université de Toulouse, CNRS, INPT, UPS
Toulouse, France
fadel@laplace.univ-tlse.fr

Marc Bodson
Electrical and Computer Engineering
University of Utah
Salt Lake City, Utah, USA
bodson@eng.utah.edu

***Abstract*—The main novelty of this paper is to introduce a new real-time optimized control allocation (CA) method of the currents scalable to any modular multilevel converter (MMC). It can be adapted to an MMC of any number of phases and submodules (SM) without having to undergo changes in the control algorithm. First the scalable state-space model of the MMC currents is presented end than, this minimal order model is used to develop the scalable current control allocation method. The control allocation is computed by fast real-time optimization using linear programming and quadratic programming algorithms. Three control allocation methods are Hardware-In-the-Loop tested for polyphase AC systems from 3 up to 101 phases, showing their ability to guarantee the current reference tracking as well as the scalability of the tracking performance. A comparison between the resolution methods highlights the benefits and pitfalls of each.**

***Index Terms*—Scalable Control, Scalable Model, Current Control, Control Allocation, Fast Real-Time Optimization, MMC, Online Optimization**

I. Introduction

Power converters with large number of switches are now widespread. The design of control laws that apply independently of the size of the converter is desirable. The article develops control allocation methods that can be used to meet this objective.

A. Control Allocation: from aeronautics to a diversification of the application fields

The objective of allocation control (CA) methods is to take advantage of the multiplicity of control variables in order to optimally operate the system under consideration. First developed in the aeronautical domain [1], [2], allocation methods were intended to take advantage of redundant actuators during the operation of an aircraft. As the application fields of these methods develop and diversify [3]–[8], they have now reached the field of electrical engineering [9], [10], the research field of which the proposed paper is part.

B. Objective of the research work

The objective of the research project is to develop allocation control methods for electrical systems with a large number of switches (i.e. a large number of control variables) of the modular multilevel converter (MMC) type. The work proposed in this paper aims at presenting the results of the exploration of this research axis. The control of the MMC has two main objectives: ensuring the current reference tracking as well as the capacitor voltage balancing [11], [12]. The study proposed here focuses on the first objective although the second one is still ensured to guarantee proper operation of the MMC. The implemented control architecture is presented in Fig. 1 where I_h^{ref}, I_s^{ref}, $\mathbf{I_c^{ref}}$ and $\mathbf{I_o^{ref}}$ are the different current references (detailed after (1)), $\mathbf{U_{HL}}$ is the control vector for the currents (detailed in (5)), v_C^{ref} is the capacitor voltage reference which is the same for all capacitors and V_C is the matrix containing all the capacitor voltages. The remaining notations are detailed in Section III.

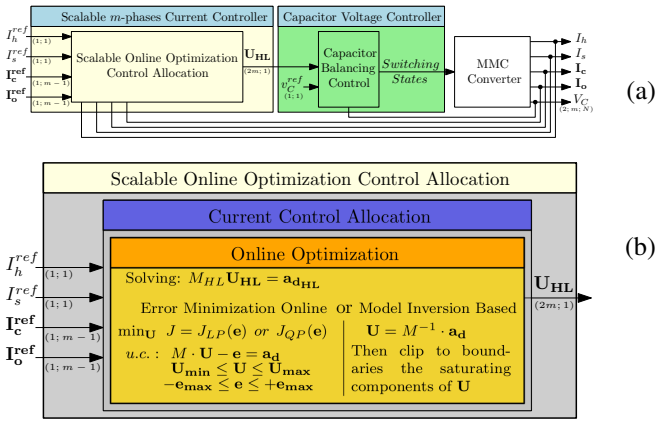

Fig. 1. MMC control architecture: (a) current control outer loop and capacitor voltage active-balancing control inner loop, (b) zoom on the current control loop.

C. Novelty of the proposed work

Since the appearance of the MMC [13], [14], with the objective to control the converted power, work has been carried out to design control laws of the currents flowing within the MMC. Classical methods 1) such as Proportional-Integral (PI) or Proportional-Resonant (PR) [11], [15], [16] first appeared and then more advanced methods 2) such as Internal Model

Control (IMC) [17], Sliding Mode Control (SMC) [12], Pole Placement Control (PCC) [12] were developed, but also methods derived from an optimization process 3) such as the Linear Quadratic Regulator (LQR) [18], but also the Model Predictive Control (MPC) [19].

Compared to the control methods 1) and 2) the CA proposed here implements a real-time optimization process aiming at optimally operating the control variables, which is not guaranteed by ad-hoc control laws. Compared to the methods 3) which are methods implementing an optimization, CA allows to perform a much faster optimization in real time at each computational step in order to adapt quickly to the evolution of the system state by determining the best value to allocate to the control. More recently, the Control Allocation (CA) using linear programming (LP) [20] has been applied to the MMC, but the current control method developed here is more general than in this study, it is scalable, takes into account the control of the common mode current and the possibility of having an active AC load with a different control architecture (see Fig. 1) which uses the LP, but also the quadratic programming (QP) and the model inversion based (MIB) CA.

Compared to previous works, the main novelty is the scalability of the proposed control method: the generalized scalable state-space model of the currents previously developed [21], [22] is reviewed in Section II, making it possible to formulate, in Section III-A, an online optimization CA algorithm also scalable to an MMC having any number of phases and submodules (SM), whatever the nature of the AC load and the presence of a common mode current. A major novelty consists in the different CA methods implemented, focusing on current control: 1) MIB in Section III-B, 2) LP in Section III-C and 3) QP in Section III-D. Finally, the paper shows the performance of the proposed control allocation to ensure the tracking of the current reference and its scalability to a high number of phase AC systems, using a Hardware-In-the-Loop (HIL) test procedure in Section IV.

II. Scalable Current State-Space Model

The CA method is based on predicting the behavior of the system to be controlled. The goal being to control the MMC, at least two control objectives are to be ensured: 1) current control, 2) voltage capacitor balancing. This article focuses on the first one. In order to deal with the second objective, methods already available in the literature are taken advantage of [23], [24]. The two control objectives are then ensured by the control architecture detailed on Fig. 1 which implements two nested loops, the inner loop - Low-Level Control (LLC) - ensures the capacitor voltage balancing while the outer loop - High-Level Control (HLC) - ensures the current reference tracking. Thus, a model describing the dynamic behavior of the currents is necessary in order to develop the control allocation. In previous work, the authors developed a scalable state-space model of the MMC for polyphase systems [21], [22] in order to be able to control the currents in an MMC of any number of phases and SMs by operating their control variables which are the arm voltages of the MMC. This state-space model is built from the following differential system where m is the number of AC phases [22]:

$$\begin{cases} L_h^{eq}\dot{I}_h = -R_h^{eq} I_h - \frac{1}{2}N_\Sigma(m)\left(\mathbf{V_{p,y}}+\mathbf{V_{n,y}}\right) \\ \qquad\qquad +N_\Sigma(2)\mathbf{V_x} - N_\Sigma(m)\mathbf{V_y} - V_{n_{AD}} \\ L_s^{eq}\dot{I}_s = -R_s^{eq} I_s - \frac{1}{2}N_\Sigma(m)\left(\mathbf{V_{p,y}}-\mathbf{V_{n,y}}\right) + [1\ 0]N_\Delta(2)\mathbf{V_x} \\ L_c^{eq}\dot{\mathbf{I}}_\mathbf{c} = -R_c^{eq}\mathbf{I_c} - \frac{1}{2}N_\Delta(m)\left(\mathbf{V_{p,y}}-\mathbf{V_{n,y}}\right) \\ L_o^{eq}\dot{\mathbf{I}}_\mathbf{o} = -R_o^{eq}\mathbf{I_o} - \frac{1}{2}N_\Delta(m)\left(\mathbf{V_{p,y}}+\mathbf{V_{n,y}}\right) - N_\Delta(m)\mathbf{V_y} \end{cases} \tag{1}$$

where, from a high-level point-of-view, there are at most four types of currents that can appear during the operation of the MMC: $I_h \in \mathbb{R}$ si the common mode current represented by i_h on Fig. 2, $I_s \in \mathbb{R}$ is the DC source current which is $(i_p - i_n)/2m$ on the same figure, $\mathbf{I_c} = [i_{c_{y_1}}, \ldots, i_{c_{y_m}}]^T \in \mathbb{R}^m$ is the circulating current vector with $i_{c_y} = (i_{p,y} - i_{n,y})/2 - I_s$ is the circulating current components, and $\mathbf{I_o} = [i_{o_{y_1}}, \ldots, i_{o_{y_m}}] \in \mathbb{R}^m$ the AC load output current with $i_{o_y} = i_y/2 - I_h$ the output current components. The behavior of these different currents is determined by the voltage across each arm of the MMC ($v_{x,y}$, $x \in \{p, n\}$ and $y \in \{y_1, \ldots, y_m\}$), the DC bus voltage (represented by v_p and v_n), and the AC voltages (v_{y_1} to v_{y_m}). Those voltages are gathered into the following vectors: $\mathbf{V_{p,y}} = [v_{p,y_1}, \ldots, v_{p,y_m}]^T \in \mathbb{R}^m$, $\mathbf{V_{n,y}} = [v_{n,y_1}, \ldots, v_{n,y_m}]^T \in \mathbb{R}^m$, $\mathbf{V_x} = [v_p, v_n]^T \in \mathbb{R}^2$, $\mathbf{V_y} = [v_{y_1}, \ldots, v_{y_m}]^T \in \mathbb{R}^2$. Equivalent resistance and inductance parameters are defined as:

$$\begin{cases} R_h^{eq} = mR_s + R + 2R_o \text{ and } L_h^{eq} = mL_s + L + 2L_o \\ R_s^{eq} = mR_s + R \text{ and } L_s^{eq} = mL_s + L \\ R_c^{eq} = R \text{ and } L_c^{eq} = L \\ R_o^{eq} = R + 2R_o \text{ and } L_o^{eq} = L + 2L_o \end{cases} \tag{2}$$

and the remaining parameters are:

$$\begin{cases} N_\Sigma(m) = \frac{1}{m}[1, \ldots, 1] \in \mathcal{M}_{1,m}(\mathbb{R}) \\ N_\Delta(m) = \frac{1}{m}[m\mathbb{I}_m - \mathbb{J}_m] \in \mathcal{M}_m(\mathbb{R}) \end{cases} \tag{3}$$

where $\mathbb{I}_m$ is the identity matrix of size m, $\mathbb{J}_{a,b}$ is the $(a \times b)$ matrix filled with $1's$, and $\mathbb{J}_m = \mathbb{J}_{m,m}$.

The differential system (1) can then be derived into a minimal state-space representation [22] whose accuracy for control has been proven:

$$\begin{cases} \dot{\tilde{\mathbf{X}}}_\mathbf{HL} = \tilde{A}_{HL}\tilde{\mathbf{X}}_\mathbf{HL} + \tilde{B}_{HL}\mathbf{U_{HL}} + \tilde{\mathbf{E}}_\mathbf{HL} \\ \tilde{\mathbf{Y}}_\mathbf{HL} = \tilde{C}_{HL}\tilde{\mathbf{X}}_\mathbf{HL} \end{cases} \tag{4}$$

where the matrices of the model are defined as:

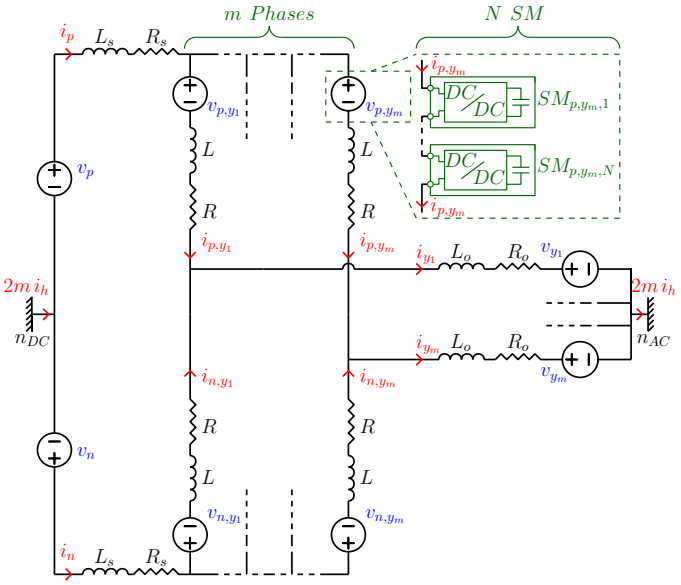

Fig. 2. Electrical diagram of the MMC with m phases and N SMs per arm

$$\tilde{A}_{HL}=\begin{bmatrix} -\frac{R_h^{eq}}{L_h^{eq}} & & & \\ & -\frac{R_s^{eq}}{L_s^{eq}} & & \\ & & -\frac{R_c^{eq}}{L_c^{eq}}\mathbb{I}_{m-1} & \\ & & & -\frac{R_o^{eq}}{L_o^{eq}}\mathbb{I}_{m-1} \end{bmatrix} \in \mathcal{M}_{2m}(\mathbb{R})$$

$$\tilde{B}_{HL}=-\frac{1}{2}\begin{bmatrix} N_\Sigma(m)/L_h^{eq} & N_\Sigma(m)/L_h^{eq} \\ N_\Sigma(m)/L_s^{eq} & -N_\Sigma(m)/L_s^{eq} \\ \gamma\cdot N_\Delta(m)/L_c^{eq} & -\gamma\cdot N_\Delta(m)/L_c^{eq} \\ \gamma\cdot N_\Delta(m)/L_o^{eq} & \gamma\cdot N_\Delta(m)/L_o^{eq} \end{bmatrix} \in \mathcal{M}_{2m}(\mathbb{R})$$

$$\tilde{C}_{HL}=\mathbb{I}_{2m}$$

$$\mathbf{U_{HL}}=[\mathbf{V_{p,y}},\mathbf{V_{n,y}}]^T\in\mathbb{R}^{2m}$$

$$\tilde{\mathbf{E}}_{\mathbf{HL}}=\begin{bmatrix} N_\Sigma(2)/L_h^{eq} \\ [1\ \ 0]\cdot N_\Delta(2)/L_s^{eq} \\ 0 \\ 0 \end{bmatrix}\mathbf{V_x}+\begin{bmatrix} -N_\Sigma(m)/L_h^{eq} \\ 0 \\ 0 \\ -\gamma\cdot N_\Delta(m)/L_o^{eq} \end{bmatrix}\mathbf{V_y} + \begin{bmatrix} -1/L_h^{eq} \\ 0 \\ 0 \\ 0 \end{bmatrix} V_{n_{AD}} \in \mathbb{R}^{2m}$$

$$\gamma=\begin{bmatrix}\mathbb{I}_{m-1} & \mathbb{O}_{m-1,1}\end{bmatrix}\in\mathcal{M}_{m-1,m}(\mathbb{R}) \tag{5}$$

The command is digital and will be executed at the sampling period T_s, so (4) is discretized into:

$$\begin{cases}\tilde{\mathbf{X}}_{\mathbf{HL}}(\mathbf{k+1})=\tilde{F}_{HL}\tilde{\mathbf{X}}_{\mathbf{HL}}(\mathbf{k})+\tilde{G}_{HL}\mathbf{U_{HL}}(\mathbf{k})+\tilde{H}_{HL}\tilde{\mathbf{E}}_{\mathbf{HL}}(\mathbf{k}) \\ \tilde{\mathbf{Y}}_{\mathbf{HL}}(\mathbf{k})=\tilde{C}_{HL}\tilde{\mathbf{X}}_{\mathbf{HL}}(\mathbf{k})\end{cases} \tag{6}$$

where $\tilde{F}_{HL}=e^{\tilde{A}_{HL}T_s}$, $\tilde{H}_{HL}=\tilde{A}_{HL}^{-1}\left(\tilde{F}_{HL}-\mathbb{I}_{2m}\right)$ and $\tilde{G}_{HL}=\tilde{H}_{HL}\tilde{B}_{HL}$. k represents the present time $t=kT_s$ and $k+1$ the next sampling time. This scalable model (1)-(6) embodies the Generalized Polyphased Full Order Current State-Space Model (GPFOCSSM) of the MMC. Since these equations do not show the number N of SMs, the GPFOCSSM is independent of N. This is due to the fact that it is a high-level model whose input variables are the voltages $\mathbf{V_{p,y}}$ and $\mathbf{V_{n,y}}$ across the arms. These voltages are composed of the SM capacitor voltages and can be expressed as a function of N. Since the high-level model does not go into this level of detail, it remains scalable to an MMC whose arms have any number of SMs since it is encapsulated in the $\mathbf{V_{p,y}}$ and $\mathbf{V_{n,y}}$ variables.

III. Control Allocation Formulation

A. Control Allocation Problem

Control allocation refers to a family of control methods that have taken different formalisms in the literature [3], [4], [8], [25], [26] but in general, the point of convergence of these approaches is the initial control problem to be treated which is written:

$$\{M\ \mathbf{U}=\mathbf{a_d}\mid \mathbf{U}_{min}\leq\mathbf{U}\leq\mathbf{U}_{max}\} \tag{7}$$

where $\mathbf{U}\in\mathbb{R}^{n_U}$ is the control vector that is to be determined, $\mathbf{a_d}\in\mathbb{R}^{n_a}$is the action vector that is desired to be reached by the system under consideration and $M\in\mathcal{M}_{n_a,n_U}(\mathbb{R})$ is the matrix emboying the effect of $\mathbf{U}$ on the system to be controlled. The objective of solving (7) is to determine the command $\mathbf{U}$ allowing the system to reach $\mathbf{a_d}$ while taking into account the constraints on the control limits $\mathbf{U_{HL}^{min}}\leq\mathbf{U_{HL}}\leq\mathbf{U_{HL}^{max}}$. This resolution can be done by different methods [3]–[5], [26], historically it is the model-inversion-based (MIB) methods that appeared first [25] then it was the turn of the online optimization methods like the error minimization online (EMOn) [4] and finally the offline optimization methods like error minimization offline (EMOff) with real-time adaptation [5]. For the step presented in this article, the formulations will be made for the MIB and EMOn methods.

To achieve the control objective $\mathbf{Y_{HL}(k)}$ will have to follow its reference $\mathbf{Y_{HL}^{ref}(k)}$ with given closed-loop dynamics specified by the desired pole vector $P_{HLC}=p_{cc}\cdot[1,\ldots,1]^T\in\mathbb{R}^{2m}$, where p_{cc} is defined in Table I for the tests. A reference model to follow can then be defined:

$$\mathbf{Y_{HL}(k+1)}=F_{HL}^{+}\mathbf{Y_{HL}(k)}+G_{HL}^{+}\mathbf{Y_{HL}^{ref}(k)} \tag{8}$$

where $A_{HL}^{+}=diag(P_{HLC})$, $B_{HL}^{+}=-A_{HL}^{+}$ in order to have a unit static gain, $F_{HL}^{+}=e^{A_{HL}^{+}T_s}$ and $G_{HL}^{+}=(A_{HL}^{+})^{-1}\left(F_{HL}^{+}-\mathbb{I}_{2m}\right)B_{HL}^{+}$. The natural behavior of the system puts forward by (6):

$$\begin{aligned}\mathbf{Y_{HL}(k+1)}=\tilde{C}_{HL}\tilde{F}_{HL}\tilde{\mathbf{X}}_{\mathbf{HL}}(\mathbf{k})+\tilde{C}_{HL}\tilde{G}_{HL}\mathbf{U_{HL}}(\mathbf{k}) \\ +\tilde{C}_{HL}\tilde{H}_{HL}\tilde{\mathbf{E}}_{\mathbf{HL}}(\mathbf{k})\end{aligned} \tag{9}$$

In order to ensure the reference model tracking, $\mathbf{U_{HL}(k)}$ must satisfy at any time k the equality between (8) and (9), thus:

$$\begin{aligned}\tilde{C}_{HL}\tilde{G}_{HL}\mathbf{U_{HL}(k)} = F^{+}_{HL}\mathbf{Y_{HL}(k)} + G^{+}_{HL}\mathbf{Y^{ref}_{HL}(k)} \\ -\tilde{C}_{HL}\left(\tilde{F}_{HL}\tilde{\mathbf{X}}_{\mathbf{HL}}(\mathbf{k}) + \tilde{H}_{HL}\tilde{\mathbf{E}}_{\mathbf{HL}}(\mathbf{k})\right)\end{aligned} \tag{10}$$

This can be directly put into the form of (11):

$$M_{HL}\cdot\mathbf{U_{HL}} = \mathbf{a_{d_{HL}}} \tag{11}$$

where $M_{HL} = \tilde{C}_{HL}\tilde{G}_{HL} = \tilde{G}_{HL} \in \mathcal{M}_{2m}(\mathbb{R})$ and $a_{d_{HL}} = F^{+}_{HL}\mathbf{Y_{HL}(k)} + G^{+}_{HL}\mathbf{Y^{ref}_{HL}(k)} - \tilde{C}_{HL}\left(\tilde{F}_{HL}\tilde{\mathbf{X}}_{\mathbf{HL}}(\mathbf{k}) + \tilde{H}_{HL}\tilde{\mathbf{E}}_{\mathbf{HL}}(\mathbf{k})\right)$. Since the allocation equation (7) has been established for the case of current control in the MMC by (11), the objective of the next three sections will be to implement a formalization suitable for the MIB and EMOn control allocation methods for current control.

B. Model-inversion-based (MIB) formulation

The MIB formulation implemented here consists in a simple inversion of (11). At each sampling period the control will be computed as follows:

$$\mathbf{U_{HL}} = M^{-1}_{HL}\mathbf{a_{d_{HL}}} = \tilde{G}^{-1}_{HL}\mathbf{a_{d_{HL}}} \tag{12}$$

$\tilde{G}_{HL}$ is square and its determinant remains nonzero as long as the inductances are different from infinity which will always be the case. However constraints on the control are part of the allocation problem to solve, in the event that any of the components of $\mathbf{U_{HL}}$ calculated by (12) exceed its lower limit $\mathbf{U^{min}_{HL}}$ or upper limit $\mathbf{U^{max}_{HL}}$, it will be clipped to its nearest limit.

C. Error minimization online (EMOn) formulation for LP

The objective of the allocation is to find $\mathbf{U_{HL}}$ that verifies (11). However $\mathbf{U_{HL}}$ is constrained to stay between $\mathbf{U^{min}_{HL}}$ and $\mathbf{U^{max}_{HL}}$, so equation (11) cannot always be satisfied. A deviation variable $\mathbf{e}$ is therefore introduced:

$$\mathbf{e} = \tilde{G}_{HL}\cdot\mathbf{U_{HL}} - \mathbf{a_{d_{HL}}} \tag{13}$$

In order to solve (11) the optimization will aim to cancel $\mathbf{e}$ and thus minimize a criterion depending on $\mathbf{e}$ under the constraint of having $\mathbf{U^{min}_{HL}} \leq \mathbf{U_{HL}} \leq \mathbf{U^{max}_{HL}}$. In the framework of linear optimization J takes the form of a linear criterion hence the choice of $l1$-norm:

$$\begin{cases} \min_{\mathbf{U_{HL}},\mathbf{e}} J_{LP} = |\mathbf{e}| = \sum_{i=1}^{n_a}|e_i| \\ \text{under the constraints } (u.c.): \\ \tilde{G}_{HL}\cdot\mathbf{U_{HL}} - \mathbf{e} = \mathbf{a_{d_{HL}}} \\ \mathbf{U^{min}_{HL}} \leq \mathbf{U_{HL}} \leq \mathbf{U^{max}_{HL}} \\ -\mathbf{e_{max}} \leq \mathbf{e} \leq \mathbf{e_{max}} \end{cases} \tag{14}$$

where $\mathbf{e_{max}}$ is an upper limit on the achievable error, here: $\mathbf{e_{max}} = \max(abs(\mathbf{a_{d_{HL}}}))\cdot[1\ldots1]^T \in \mathbb{R}^{2m}$. Other ways to define $\mathbf{e}$ boundaries have already been used [4]. Real-time LP algorithms are built on methods to solve the formulation (15):

$$\begin{cases} \min_{\mathbf{x}} J_{LP} = \mathbf{c}^T\mathbf{x} \\ u.c.: \\ A\cdot\mathbf{x} = \mathbf{b} \\ \mathbf{0} \leq \mathbf{x} \leq \mathbf{x_{max}} \end{cases} \tag{15}$$

To adopt the formulation (15), $\mathbf{e}$ is decomposed into $\mathbf{e} = \mathbf{e}^{+} - \mathbf{e}^{-}$ with $\mathbf{e}^{+}, \mathbf{e}^{-} \geq 0$ and a change of variable is made on $\mathbf{U}$: $\mathbf{U} = \overline{\mathbf{U}} - \mathbf{U_{min}}$. Thus, (14) takes the form of (15) whose parameters are then:

$$\begin{aligned} &\mathbf{x} = \left[\overline{\mathbf{U_{HL}}} \quad \mathbf{e}^{+} \quad \mathbf{e}^{-}\right]^T \in \mathbb{R}^{6m} \\ &\mathbf{c}^T = \left[\mathbb{O}_{1,2m} \quad 1\ldots1 \quad 1\ldots1\right] \in \mathbb{R}^{6m} \\ &A = \left[\tilde{G}_{HL} \quad -\mathbb{I}_{2m} \quad +\mathbb{I}_{2m}\right] \in \mathcal{M}_{2m,6m}(\mathbb{R}) \\ &\mathbf{b} = \left[\mathbf{a_{d_{HL}}} - \tilde{G}_{HL}\cdot\mathbf{U^{min}_{HL}}\right] \in \mathbb{R}^{2m} \\ &\mathbf{x_{max}} = \left[\mathbf{U^{max}_{HL}} - \mathbf{U^{min}_{HL}} \quad \mathbf{e_{max}} \quad \mathbf{e_{max}}\right] \in \mathbb{R}^{6m} \end{aligned} \tag{16}$$

The size of the elements in (16) depends on the number of phases, which highlights the scalability of the control allocation method that will be solved using LP in real time.

It is important to note that it is possible to take into account a weighting of the control objectives represented by (7), in general, and by (11) in the case of the converter. Indeed, it is possible to multiply a line of M_{HL}, and the corresponding line of $\mathbf{a_{d_{HL}}}$, by the same factor to give them more or less importance in the global criterion J. For example, with the converter, if one wishes to give more importance to the control objective of tracking $\mathbf{I^{ref}_{o}}$ and therefore less importance to the tracking of other currents: lines 3 to $m+2$ of M_{HL} and $\mathbf{a_{d_{HL}}}$ can be multiplied by the weight w_o with $w_o > 1$ in order to give more importance to tracking the reference output currents. Matrices M_{HL} and $\mathbf{a_{d_{HL}}}$ are redefined and no changes need to be made to the algorithm solving (15) (or (17) for the QP) because they are already contained in the matrices A and $\mathbf{b}$ of (16) (or (19) for the QP).

D. Error minimization online (EMOn) formulation for QP

Real-time QP algorithms are built on methods for solving the formulation (17):

$$\begin{cases} \min_{\mathbf{x}} J_{QP} = \frac{1}{2}\mathbf{x}^T H\mathbf{x} + \mathbf{c}^T\mathbf{x} + f \\ u.c.: \\ A\cdot\mathbf{x} = \mathbf{b} \\ \mathbf{x_{min}} \leq \mathbf{x} \leq \mathbf{x_{max}} \end{cases} \tag{17}$$

Compared to LP, QP offers the choice of a quadratic criterion and the possibility of having negative boundaries.

$$\begin{cases} \min_{\mathbf{U_{HL}},\mathbf{e}} J_{QP} = ||\mathbf{e}||^2 = \sum_{i=1}^{n_a} e_i^2 \\ u.c.: \\ \tilde{G}_{HL}\cdot\mathbf{U_{HL}} - \mathbf{e} = \mathbf{a_{d_{HL}}} \\ \mathbf{U^{min}_{HL}} \leq \mathbf{U_{HL}} \leq \mathbf{U^{max}_{HL}} \\ -\mathbf{e_{max}} \leq \mathbf{e} \leq \mathbf{e_{max}} \end{cases} \tag{18}$$

The adoption of the form (17) by (18) is more direct with QP:

$$\begin{aligned}
&\mathbf{x} = \begin{bmatrix}\mathbf{U_{HL}} & \mathbf{e}\end{bmatrix}^T \in \mathbb{R}^{4m} \\
&H = 2\begin{bmatrix}\mathbb{O}_{2m} & \\ & \mathbb{I}_{2m}\end{bmatrix} \in \mathcal{M}_{4m}(\mathbb{R}) \\
&\mathbf{c}^T = \begin{bmatrix}\mathbb{O}_{1,4m}\end{bmatrix} \in \mathbb{R}^{4m} \qquad f = 0 \\
&A = \begin{bmatrix}\tilde{G}_{HL} & -\mathbb{I}_{2m}\end{bmatrix} \in \mathcal{M}_{2m,4m}(\mathbb{R}) \\
&\mathbf{b} = \begin{bmatrix}\mathbf{a_{d_{HL}}}\end{bmatrix} \in \mathbb{R}^{2m} \\
&\mathbf{x_{min}} = \begin{bmatrix}\mathbf{U_{min}} & -\mathbf{e_{max}}\end{bmatrix} \in \mathbb{R}^{4m} \\
&\mathbf{x_{max}} = \begin{bmatrix}\mathbf{U_{max}} & +\mathbf{e_{max}}\end{bmatrix} \in \mathbb{R}^{4m}
\end{aligned} \tag{19}$$

The size of the elements in (19) depends on the number of phases, which emphasizes the scalability of the control allocation method that will be solved using QP in real time. Note that the size of the LP is larger than that of the QP in the context of the MMC current control which is due to the possibility, in QP, to have negative decision variables.

The online optimization for solving (15) will be done by a simplex algorithm [4] (EMOn LP SX), whereas (17) will be solved by an active-set algorithm [27] (EMOn QP AS).

IV. HIL Test Procedure

The procedure to test the online optimization allocation methods aims to show the scalability of the different formulations to the number of phases and in particular to show their capability to ensure the current reference tracking with good performance.

Since the focus is on the behavior of the currents in closed-loop, the voltage control inner loop will maintain capacitor voltages at their nominal value while the control of current is under scrutiny in transient and steady-state conditions. Fig. 4 shows the current and capacitor voltage response to several steps in output current reference. The AC system has 7 phases. In order to ease the reading of Fig. 4, references for phases $\#2$ to $\#7$ are the same as in phase $\#1$ but shifted by $2\pi/7$ rad between each phase.

The tests are performed with an HIL system shown in Fig. 3, with parameters as well as those of the system and hardware given in the Table I.

A. HIL test results of the implemented CA EMOn QP

As the results of the different allocation methods are quite similar as will be seen in the next section IV-B, it was chosen to first show the detailed results for only one of the three CA implementations: the one using online QP.

In Fig 4, an excellent current control reference tracking is observed, since the maximum control error on the different types of currents is smaller than 37 mA (i.e. less than 2.5%) in steady-state. Moreover, after a step in output current reference, the 5% settling time is roughly 1 ms, which corresponds to the expectation with controllers tuned for a 500 Hz bandwidth in closed-loop. Overall, the results prove that the use of the control-oriented scalable state-space model for the development of a current online optimization CA algorithm ensures a very good control performance in transient as well as in steady-state conditions.

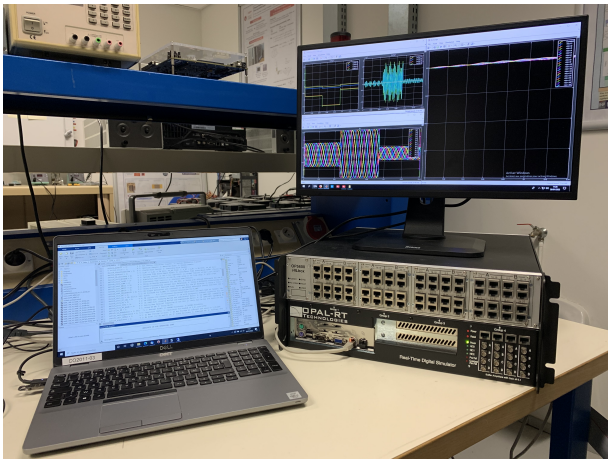

Fig. 3. Hardware-In-the-Loop test setup with the Opal-RT 5600 HIL box at the LAPLACE laboratory.

TABLE I
Closed-Loop, MMC & Opal-RT HIL Box Parameters

Meaning	Symbol	Value
MMC Hardware Parameters		
Bus voltage	V_{DC}	600 V
Half-bus voltage	$v_p = -v_n$	$V_{DC}/2 = 300$ V
Bus resistance and inductance	R_s, L_s	50 mΩ, 2 mH
Switching frequency and period	f_s, T_s	4 kHz, 250 µs
Arm resistance and inductance	R, L	10 mΩ, 5 mH
AC active voltage	$\hat{V}_{AC}$	150 V
AC grid frequency and period	f_o, T_o	50 Hz, 20 ms
AC grid pulsation	ω_o	$2\pi f_o \simeq 314$ rad/s
AC load resistance and inductance	R_o, L_o	40 Ω, 5 mH
Opal-RT 5600 HIL Box Parameters		
CPU Type	–	Intel Xeon
CPU Clock	–	3.00 GHz
CPU Cache / RAM	–	11.6 Gb / 64 Gb
HIL time step	T_{step}	$T_s/10 = 25$ µs
HIL data logging duration	t_{log}	$7 \cdot T_o = 140$ ms
Closed-Loop Parameters		
Current control poles, bandwidth	p_{cc}, f_{bw}	-3142 rad/s, 500 Hz
Control sampling time	T_c	250 µs

B. Comparison of the different CA formulations implemented

The tests performed for the EMOn QP implementation of the CA presented in the previous section are also performed for the other two implementations: MIB and EMOn LP. The test presented in the previous section IV-A is done for $m = 7$ phases, this same test is done for m ranging from 3 to 101 and this for the three algorithmic implementations of the CA. In total, this results in 294 tests. For each test, the deviation between the reference of each current and the current is evaluated as well as the computation time needed for the CA algorithm to run in real time. For a given test, the average value of the deviation over the entire test duration is computed as follows:

$$\epsilon_o = \left\langle \frac{||\mathbf{I_o^{ref}} - \mathbf{I_o}||}{||\mathbf{I_o^{ref}}||} \right\rangle_{t_{end}} \tag{20}$$

First, on Fig. 5 the logarithmic scale is used for a better readability, however in linear scale it is observed that the computation time of the three implementations of CA

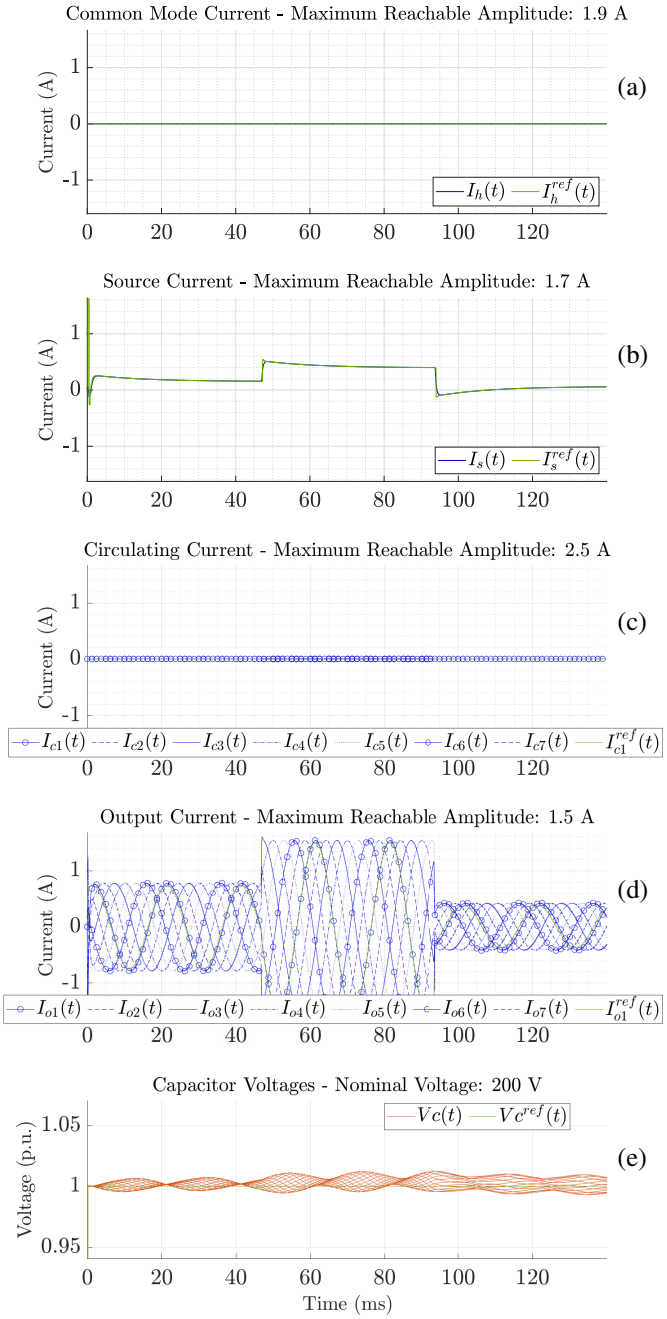

Fig. 4. Closed-loop response of the system to changes in the output current reference. (a) Common mode current, (b) Source current, (c) Circulating current, (d) Output current, (e) Capacitors voltages.

increases quadratically according to the number of phases. This is explained by the fact that the size of M_{HL} and $\mathbf{a_{d_{HL}}}$ increase with the number of phases (as the state-space model does); thus, the complexity of the control allocation algorithm also increases. Then, Fig. 5 highlights the fact that the output current control error remains constant as the phase number increases, which is a major result: the MMC control allocation performance is scalable. Therefore, Fig. 5 presents two strong results of the current allocation control methods introduced

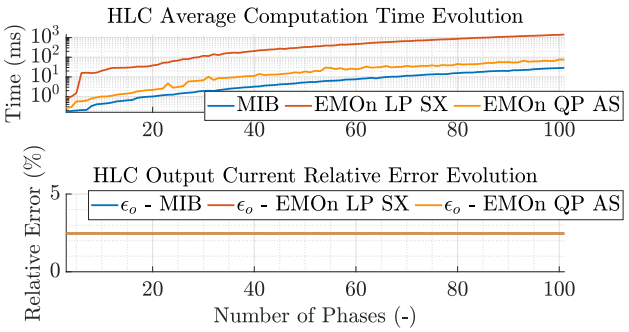

Fig. 5. Evolution of the control allocation characteristics vs. the number of phases.

here: 1) these methods are readily scalable to a large number of phases, 2) the accuracy of the current tracking - and in particular of the output current on Fig. 5 - is of very good quality and remains constant whatever the number of phases of the polyphase AC system. Note that the three implementations of the CA all give good control performances with each a different computation time making all three good candidates to ensure current control in the MMC for less than 10 phases in the AC system but for a larger number of phases, one would rather use the MIB or the EMOn QP AS.

V. Conclusions

The control-oriented state-space model of the currents scalable to an MMC of any size, whose accuracy for control has already been proven, was first presented. The main contribution was the introduction of three formulations of control allocation, including two formulations by fast online optimization, with the objective of guaranteeing the control of the four types of currents flowing through the MMC during its operation. A major novelty lies in the scalability of the proposed methods both in terms of mathematical formulation and control performance. Indeed, tests in HIL have shown the ability of the allocation methods to ensure good quality current reference tracking and has shown that this performance is scalable to a large number of AC phases. Through this study a comparison of three CA methods in terms of computation time, current control performance and implementation complexity was conducted. For a number of phases less than 10, the computation time of the three methods make them all candidates to control currents, however as the number of phases increases, the MIB and EMOn QP AS methods become more interesting. Nonetheless, the EMOn methods are more complex to implement than the presented MIB because of the optimization algorithm to be programmed. Thus, depending on the polyphase AC system to be controlled at the output of the MMC and on the real time computational resources, a trade-off between these CA methods will have to be carried out.

As an outcome of the work presented in the paper, new capabilites are now made possible:

- Thanks to the scalable state-space model, it is possible to design generic current control algorithms for MMCs. Thus, to control a given MMC, it will be sufficient to specify to the algorithm the parameters of the MMC, of the AC network, and of the DC bus without having to change the control algorithm.
- It is now possible to develop current control algorithms for MMCs - of any number of phases and submodules, whatever the nature of the AC load and the presence or absence of a common mode current - using the same online optimization control allocation algorithm that is scalable without having to undergo changes in the code. As the control allocation scales up, control performance remain the same.
- It is now possible to use three control allocation methods: model-inversion-based, error minimization online using linear programming and error minimization online using quadratic programming to control the currents in the MMC. The choice of the method is made according to the number of phases and the available computational resources.

REFERENCES

[1] E. G. Ryanski, "Experimental Experience at Calspan," in *Restructurable Controls*, Aug. 1983, pp. 99–114, nasa Conference Publication 2277.

[2] T. B. Cunningham, "Robust Reconfiguration for High Reliability and Survivability for Advanced Aircraft," in *Restructurable Controls*, Aug. 1983, pp. 43–80, nasa Conference Publication 2277.

[3] T. A. Johansen and T. I. Fossen, "Control allocation—A survey," *Automatica*, vol. 49, no. 5, pp. 1087–1103, May 2013.

[4] M. Bodson, "Evaluation of optimization methods for control allocation," *Journal of Guidance, Control, and Dynamics*, vol. 25, no. 4, pp. 703–711, Jul. 2002.

[5] F. Liao, K. Lum, J. L. Wang, and M. Benosman, "Constrained Nonlinear Finite-Time Control Allocation," in *2007 American Control Conference*, Jul. 2007, pp. 3801–3806.

[6] S. A. Frost and M. Bodson, "Resource balancing control allocation," in *Proceedings of the 2010 American Control Conference*, Jun. 2010, pp. 1326–1331.

[7] S. S. Tohidi, Y. Yildiz, and I. Kolmanovsky, "Adaptive Control Allocation for Over-Actuated Systems with Actuator Saturation," *IFAC-PapersOnLine*, vol. 50, no. 1, pp. 5492–5497, Jul. 2017.

[8] P. Kolaric, V. G. Lopez, and F. L. Lewis, "Optimal dynamic Control Allocation with guaranteed constraints and online Reinforcement Learning," *Automatica*, vol. 122, p. 109265, Dec. 2020.

[9] A. Bouarfa, M. Bodson, and M. Fadel, "An Optimization Formulation of Converter Control and Its General Solution for the Four-Leg Two-Level Inverter," *IEEE Transactions on Control Systems Technology*, vol. 26, no. 5, pp. 1901–1908, Sep. 2018.

[10] J. Kreiss, M. Bodson, R. Delpoux, J.-Y. Gauthier, J.-F. Trégouët, and X. Lin-Shi, "Optimal control allocation for the parallel interconnection of buck converters," *Control Engineering Practice*, vol. 109, Apr. 2021.

[11] K. Sharifabadi, L. Harnefors, H.-P. Nee, S. Norrga, and R. Teodorescu, "Dynamics and control," in *Design, control, and application of modular multilevel converters for HVDC transmission systems*. IEEE, 2016, pp. 133–213.

[12] M. Zama, "Modeling and control of modular multilevel converters (MMCs) for HVDC applications," Ph.D. Thesis, Communauté Université Grenoble Alpes, 2017.

[13] R. Marquardt, "Current rectification circuit for voltage source inverters with separate energy stores replaces phase blocks with energy storing capacitors," DE Patent DE10 103 031A1, Jul., 2002.

[14] A. Lesnicar and R. Marquardt, "An innovative modular multilevel converter topology suitable for a wide power range," in *2003 IEEE Bologna Power Tech Conference Proceedings*, vol. 3, Jun. 2003.

[15] N. Serbia, "Modular multilevel converters for HVDC power stations," Ph.D. Thesis, Institut National Polytechnique de Toulouse, 2014.

[16] N. Quach, J.-H. Ko, D.-W. Kim, and E.-H. Kim, "An Application of Proportional-Resonant Controller in MMC-HVDC System under Unbalanced Voltage Conditions," 2014.

[17] Y. Li, J. Han, Y. Cao, Y. Li, J. Xiong, D. Sidorov, and D. Panasetsky, "A modular multilevel converter type solid state transformer with internal model control method," *International Journal of Electrical Power & Energy Systems*, vol. 85, pp. 153–163, Feb. 2017.

[18] E. Rakhshani, K. Rouzbehi, J. M. Escaño, and J. Rueda Torres, "Optimal Linear Control of Modular Multi-Level Converters with a Prescribed Degree of Stability," *Electric Power Components and Systems*, vol. 48, no. 1-2, pp. 30–41, Jan. 2020.

[19] B. S. Riar, T. Geyer, and U. K. Madawala, "Model Predictive Direct Current Control of Modular Multilevel Converters: Modeling, Analysis, and Experimental Evaluation," *IEEE Transactions on Power Electronics*, vol. 30, no. 1, pp. 431–439, Jan. 2015.

[20] A. Bouarfa, M. Fadel, and M. Bodson, "Optimization method based on simplex algorithm for current control of modular multilevel converters," in *2019 IEEE International Conference on Industrial Technology (ICIT)*, Feb. 2019, pp. 1220–1225.

[21] G. Le Goff, M. Fadel, and M. Bodson, "Modular Polyphased Full Order Current State-Space Model of the Modular Multilevel Converter," in *2021 IEEE 19th International Power Electronics and Motion Control Conference (PEMC)*, Apr. 2021, pp. 132–139.

[22] ——, "Scalable Control-Oriented Model of the Modular Multilevel Converter for Polyphase Systems [accepted, to appear in IEEE Transactions on Industry Applications]," 2022.

[23] R. Lizana, M. A. Perez, D. Arancibia, J. R. Espinoza, and J. Rodriguez, "Decoupled current model and control of modular multilevel converters," *IEEE Transactions on Industrial Electronics*, vol. 62, no. 9, pp. 5382–5392, Sep. 2015.

[24] M. Hagiwara and H. Akagi, "Control and Experiment of Pulsewidth-Modulated Modular Multilevel Converters," *IEEE Transactions on Power Electronics*, vol. 24, no. 7, pp. 1737–1746, Jul. 2009.

[25] W. C. Durham, "Constrained control allocation," *Journal of Guidance, Control, and Dynamics*, vol. 16, no. 4, pp. 717–725, 1993.

[26] K. A. Bordignon, "Constrained control allocation for systems with redundant control effectors," Dec. 1996, accepted: 2014-03-14T20:14:54Z Artwork Medium: BTD Interview Medium: BTD Publisher: Virginia Tech.

[27] O. Härkegård, *Backstepping and control allocation with applications to flight control*. Linköping: Univ, 2003.